ARTICLES

Skew of mantle upwelling beneath the East Pacific Rise governs segmentation

Douglas R. Toomey[1], David Jousselin[2], Robert A. Dunn[3], William S. D. Wilcock[4] & R. S. Detrick[5]

Mantle upwelling is essential to the generation of new oceanic crust at mid-ocean ridges, and it is generally assumed that such upwelling is symmetric beneath active ridges. Here, however, we use seismic imaging to show that the isotropic and anisotropic structure of the mantle is rotated beneath the East Pacific Rise. The isotropic structure defines the pattern of magma delivery from the mantle to the crust. We find that the segmentation of the rise crest between transform faults correlates well with the distribution of mantle melt. The azimuth of seismic anisotropy constrains the direction of mantle flow, which is rotated nearly 10° anticlockwise from the plate-spreading direction. The mismatch between the locus of mantle melt delivery and the morphologic ridge axis results in systematic differences between areas of on-axis and off-axis melt supply. We conclude that the skew of asthenospheric upwelling and transport governs segmentation of the East Pacific Rise and variations in the intensity of ridge crest processes.

The origin of segmentation of oceanic spreading centres is controversial. According to one point of view, along-axis differences in ridge crest processes result directly from three-dimensional mantle upwelling[1–4]. Sites of vigorous volcanic and hydrothermal activity are thus thought to overlie regions of greater magma supply. Limited knowledge of mantle structure, however, has given rise to diverging opinions on the scale of three-dimensional upwellings[2–6]. Alternatively, segmentation of ridge crest processes may be regulated by the tectonic rifting of young lithosphere[7], and thus not directly linked to the form of mantle upwelling. In this case mantle flow could be either two-dimensional[8] or three-dimensional and less obvious because of efficient along-axis transport of magma by viscous flow[9].

Along the global ridge system, the fast-spreading East Pacific Rise (EPR) between the Siqueiros and Clipperton transforms (Fig. 1) currently offers our best opportunity for understanding the relations between mantle upwelling and ridge crest processes. There are several reasons for this. This section of the EPR encompasses a full spectrum of rise axis discontinuities, including: two large-offset transform faults; large, long-lived (9° 03′ N) and small, short-lived (9° 37′ N) overlapping spreading centres (OSCs)[10–12]; and smaller-scale morphologic[3], petrologic[5,12] and seismic[6,13,14] discontinuities that are typical of fast-spreading ridge segments. Accompanying these axial discontinuities are well known along-axis variations in seafloor depth, axial high morphology[15], crustal structure and thickness[16–19], lava chemistry[5,12,20,21], and seafloor hydrothermal[22,23] and biological activity[22]. These characteristics of the EPR, including the origin of ridge crest segmentation, have been hypothesized to result from the supply of magma from the mantle.

We conducted the UNDERSHOOT experiment (our data-gathering cruise) to seismically image the crustal and mantle structure between the Clipperton and Siqueiros transforms to determine the pattern of magma delivery from the mantle to the crust. Here we present the first images of mantle structure beneath an entire ridge segment bounded by long-lived tectonic discontinuities (Fig. 1). Good image resolution allows direct comparison between the scales of segmentation observed along this section of the EPR with the physical structure of the topmost mantle. Our results allow conclusions to be drawn about the driving and controlling processes for segmentation of fast-spreading ridges.

Experiment geometry and tomographic imaging

The distribution of seismic receivers and sources used to image crustal and mantle structure is shown in Fig. 1. The experiment constrains the structure of the uppermost mantle within 4 km of the Mohorovičić discontinuity and within an area extending 15 km to either side of the rise axis and 230 km along the spreading centre. A three-dimensional model of off-axis crustal structure and thickness is used to analyse the mantle refraction data (see Supplementary Information).

The P_n data (from the wave refracted below the Moho) provide good spatial sampling of mantle structure throughout the image volume (Fig. 2a). P_n travel-time residuals plotted by azimuth reveal a $\cos 2\Theta$ pattern (Fig. 2b), a signal indicative of azimuthal seismic anisotropy. The azimuth of anisotropy (that is, the fast direction for P_n propagation) is N73°E ± 1° (see Supplementary Information). Tomographic inversions, discussed below, confirm this result. The azimuth of anisotropy is rotated 9° anticlockwise with respect to the predicted spreading direction[24] (N82°E). Plotted by rise crossing point, P_n travel-time residuals show evidence for anomalously low and variable upper-mantle velocities (Fig. 2c). The average isotropic velocity that best fits the P_n data (7.6 km s^{-1}) is less than typical upper-mantle velocities, whereas delays are greater towards the centre of the transform-bounded segment and less within 20 km of the transforms.

Tomographic inversion (see Supplementary Information) of P_n travel-time data reveals a mantle low-velocity zone (MLVZ) that is segmented on a scale comparable to tectonic offsets of the EPR (Fig. 1). The MLVZ decreases in amplitude towards each transform, in agreement with the decrease in mean P_n delays (Fig. 2c). Between transforms, the MLVZ follows two *en echelon* trends that are orthogonal to the azimuth of seismic anisotropy (Fig. 1b, green lines). The *en echelon* trends are offset in a right lateral sense and rotated

[1]Department of Geological Sciences, University of Oregon, Eugene, Oregon 97403, USA. [2]Nancy-Université, CRPG, 54501 Vandoeuvre les Nancy, France. [3]Department of Geology and Geophysics, University of Hawaii-SOEST, Honolulu, Hawaii, 96822, USA. [4]School of Oceanography, University of Washington, Seattle, Washington 98195, USA. [5]Department of Geology and Geophysics, Woods Hole Oceanographic Institution, Woods Hole, Massachusetts 02543, USA.

anticlockwise with respect to the axis of plate spreading. Owing to this azimuthal rotation, much of the MLVZ is not centred beneath the plate boundary. Beneath and immediately north of the OSC, the MLVZ steps rightward, defining a geometrically complex transitional region that connects the *en echelon* trends of the MLVZ. The transitional region, located between 9° 00′ N and 9° 18′ N, is shifted northward of the OSC itself and coincides with a region of thicker crust[18,19].

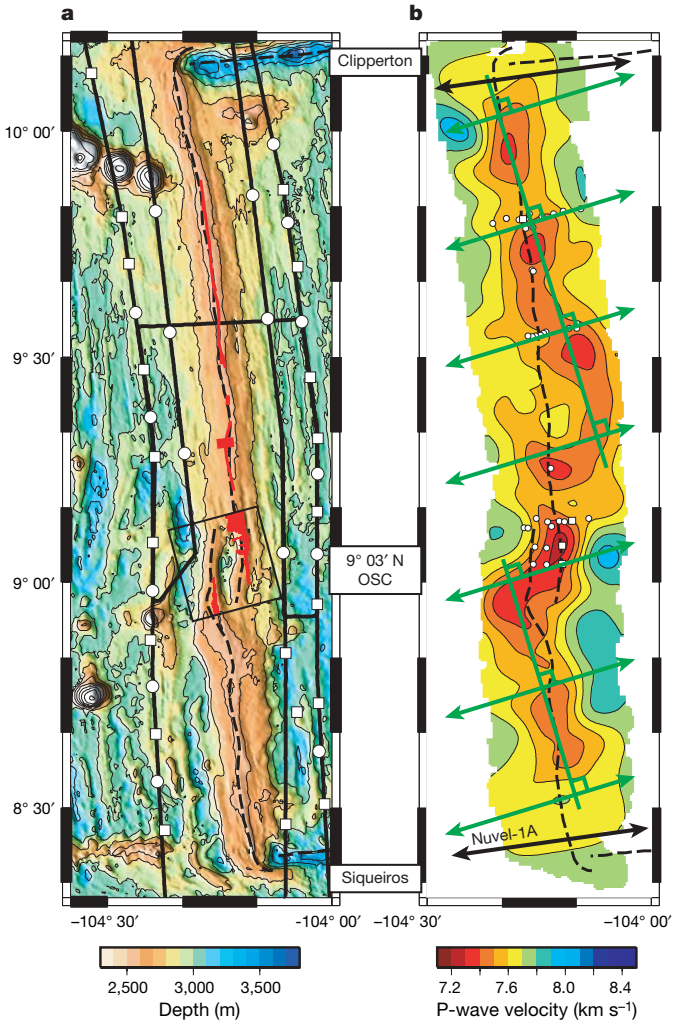

Figure 1 | Location and geometry of the seismic experiment and tomographic image of the mantle low-velocity zone (MLVZ) and orientation of mantle anisotropy. **a**, The Clipperton and Siqueiros transform faults bound the study area. Dashed lines show the location of the plate boundary. Seismic data were collected on 37 ocean-bottom receivers from the Woods Hole Oceanographic Institution. Twenty of these were Office of Naval Research, three-component seismometers (open squares) equipped with 1-Hz geophones and a hydrophone; the remaining units were ocean-bottom hydrophones (open circles). The seismic source was the RV *Maurice Ewing*'s 20-gun, 8,500-cubic-inch (139 litre) air gun array, fired at intervals of 210 s (shot spacing of 500 m) along the tracks indicated by solid black lines. Locations of axial magma chamber reflector from multichannel seismics shown in red[13,16,28]. Black box indicates the location of the three-dimensional multichannel seismics experiment. **b**, Tomographic image of mantle P-wave velocity; contour interval is 0.1 km s^{-1} and depth of section is 9 km beneath the sea floor. Green lines with arrowheads indicate azimuth of seismic anisotropy (see Figs 2b and 3); black lines with arrowheads indicate plate-spreading direction[24]. Green lines without arrowheads are perpendicular to seismic anisotropy and indicate locations of *en echelon* segments of the MLVZ. Seafloor compliance measurements are indicated by white symbols[26]; larger white squares are locations where near-Moho melt sills were detected.

North of the OSC, local minima of the MLVZ occur at intervals of approximately 25 km. Pronounced sub-axial anomalies are located near 9° 56′ N and 9° 44′ N. Equally pronounced anomalies are centred more than 10 km off-axis at 9° 32′ N and a few kilometres off-axis at 9° 15′ N. Between 9° 15′ N to 9° 35′ N the MLVZ is located 5–15 km east of the rise axis, in a region where magnetotelluric studies detect anomalously low mantle conductivities[25]. South of the OSC there is a local minima of the MLVZ near 8° 43′ N. Within our study area, the most pronounced mantle anomaly occurs beneath the eastern limb of the OSC, where several compliance measurements suggest near-Moho sills[26] and seismic imaging detects substantial amounts of melt in the lower crust[27]. The transition of the MLVZ between opposing limbs of the OSC also coincides well with a similar transition of the crustal-level axial magma chamber reflector[28] (Fig. 1).

We conducted a series of tomographic inversions for fixed models of mantle anisotropy to explore the tradeoffs between isotropic and anisotropic structure. An isotropic mantle results in a large χ-squared travel-time misfit (~6). Figure 3 shows that the data misfit is smallest

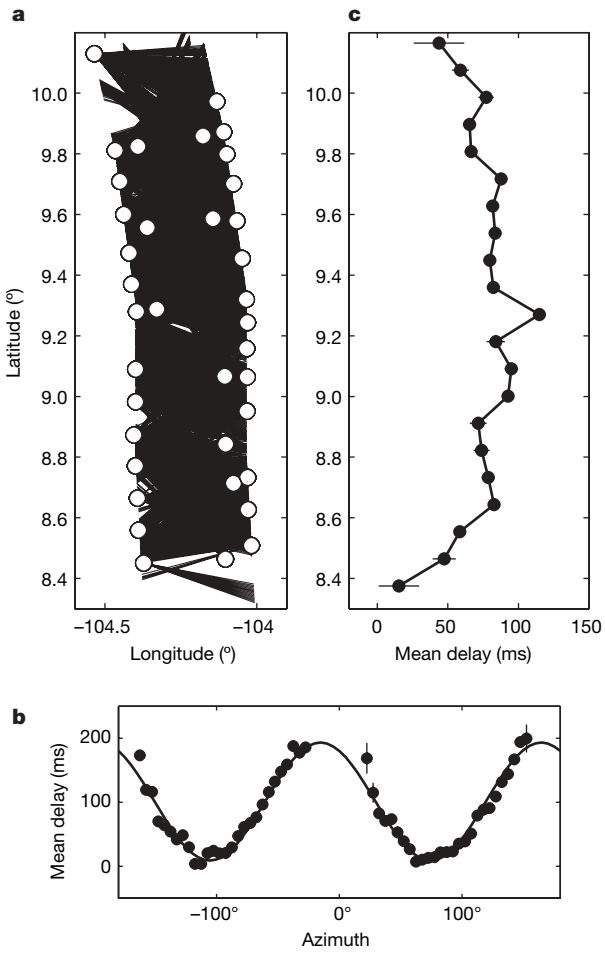

Figure 2 | Map of the distribution of seismic ray paths and mean P_n delay times versus azimuth and latitude. **a**, Map of the distribution of the 4,892 P_n ray paths used to image mantle structure. P_n data sample the mantle within about ±15 km of the rise axis. **b**, Mean P_n delay plotted by azimuth. Delays are calculated relative to an isotropic model, corrected to 40 km range and binned at intervals of 5°. Vertical bars indicate uncertainty in mean delay as determined by a Student's *t*-test (95% confidence interval). Solid line is the best-fit cos2Θ curve. The azimuth of seismic anisotropy is N73°E ± 1°. **c**, Mean P_n delay plotted by rise-axis crossing point. Delays are calculated relative to 7.8 km s^{-1}, corrected to 40 km range and have been corrected for seismic anisotropy (6% with fast axis azimuth of N73°E). Data are binned at intervals of 10 km and bars indicate uncertainty in mean delay time as determined from a Student's *t*-test (95% confidence interval).

when the azimuth of anisotropy imposed on the tomographic procedure is identical to that estimated directly from the P_n data (Fig. 2b). The data misfit is significantly larger when azimuthal anisotropy matches the predicted spreading direction. A robust result of our analysis is that both the azimuth of seismic anisotropy relative to the spreading direction and the *en echelon* trends of the MLVZ with respect to the plate boundary are rotated anticlockwise by similar amounts.

The Supplementary Information summarizes our analysis of model sensitivity and resolution and details how our current results differ from previously published studies. Therein we show that a ray-tracing error in a previous study of the 9° 03′ N OSC[29] resulted in an incorrect image.

Skew of mantle upwelling and asthenospheric flow

The isotropic component of our tomographic image constrains the distribution of melt in the topmost mantle. Regions of anomalously low seismic velocities are consistent with higher melt fractions. If melt resides in film-like geometries[30,31], then our results can be explained by the presence of 1–3% melt (see Supplementary Information); melt fractions would be greater if distributed anisotropically or if melt pockets are more spherically shaped. We attribute the MLVZ to a region of melt accumulation that lies beneath the base of newly formed oceanic crust; given the seismic wavelength, the vertical extent of this region must be several kilometres. We infer that the locus of sub-crustal melt accumulation overlies the melt production region located at depths of several tens of kilometres. The alternative, that large volumes of partially molten mantle have been transported off-axis, seems unlikely. According to this view, the axis of mantle upwelling that gives rise to decompression melting is skewed beneath the plate boundary.

The anisotropic component of our model constrains the direction of shallow mantle flow. This is because the maximum compressional wave speed for single-crystal olivine parallels the crystallographic *a* axis and deformation of mantle peridotites preferentially aligns the *a* axis in the direction of maximum shear[32,33]. Immediately beneath a spreading centre, the overturn accompanying mantle divergence generates shear strains that are many times larger than the deformation resulting from the movement of a plate over the asthenosphere[34]. We thus infer that the azimuth of seismic anisotropy beneath the spreading axis is related to the azimuth of mantle divergence. We conclude that in relation to the ridge, mantle flow is skewed by 9° with respect to the plate-spreading direction. The transport of asthenosphere away from the EPR and the axis of decompression upwelling are thus rotated anticlockwise in a coherent manner (Fig. 1).

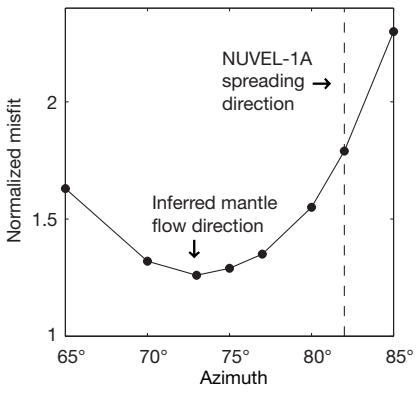

Figure 3 | Normalized data misfit following tomographic inversion versus azimuth of seismic anisotropy imposed on starting model. For each inversion, percentage (6%) and azimuth of anisotropy are held fixed. Data misfit is a minimum for an azimuth of N73°E. Misfit is significantly larger when the azimuth of anisotropy parallels the spreading direction predicted by the NUVEL-1A model[24].

The azimuthal rotation of mantle flow beneath the EPR is in the same direction as recent changes in the Euler pole for Pacific–Cocos plate motion, which has been progressing anticlockwise for the past several million years[35]. Ongoing changes in plate kinematics[35], however, are lagging behind the current direction of asthenospheric flow. We propose that the skew of mantle flow beneath the EPR is one of the driving forces for changes in plate boundary kinematics. Specifically, basal tractions imposed by mantle flow are contributing to anticlockwise changes in the spreading direction. This flow may also contribute to the transpressional and transtensional tectonics of the Clipperton and Siqueiros transforms[35], respectively (Fig. 4). The lag of the rigid plate system relative to the viscous asthenosphere may indicate that transpressive transform faults, such as the Clipperton, limit the rate at which plates adjust to changes in plate driving forces[36].

Ridge segmentation and mantle structure

Our study shows that the tectonic segmentation of the EPR correlates well with the pattern of melt delivery from the mantle to the crust. Near transforms or first-order offsets of the ridge crest[3], the increase in seismic velocities is consistent with a decrease in the amount of

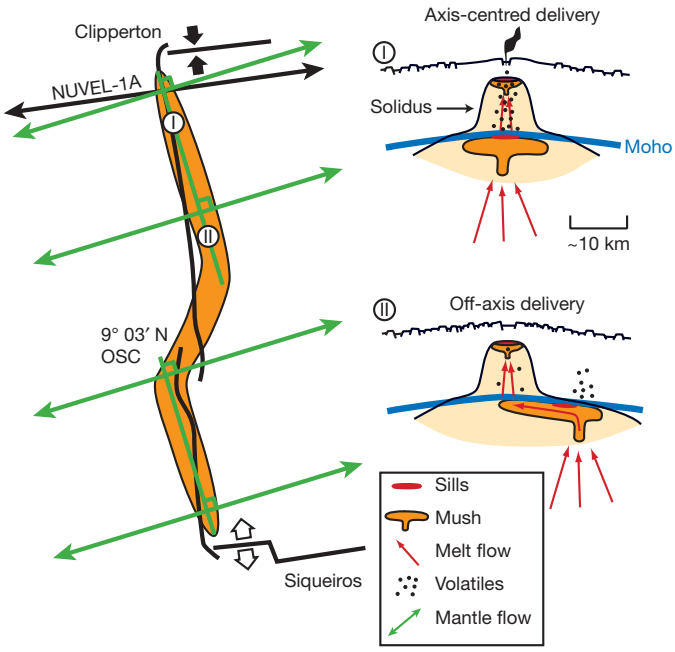

Figure 4 | Proposed model of segmentation beneath the East Pacific Rise. **a**, Map view showing plate boundary and tectonic discontinuities (solid black lines), regions of melt accumulation beneath the crust (orange area labelled 'Mush'), orientation of mantle flow (green lines with arrowheads) and trend of the *en echelon* segments of melt accumulation (green lines without arrowheads; perpendicular to mantle flow). Thin black line with arrowheads indicates NUVEL-1A spreading direction[24]. Large, paired arrows indicate regions of transpression (solid) and transtension (open) along the Clipperton and Siqueiros transform faults, respectively[35]. Circles with roman numerals indicate location of cross-sections shown in **b**. **b**, Two rise-perpendicular sections depicting magma plumbing beneath axis-centred (top) and off-axis (bottom) sites of mantle melt delivery. Above centres of melt delivery, magma accumulates at near-Moho depths, presumably within a mush-like compaction layer (orange region), with substantially lower melt concentrations in surrounding regions of the mantle. Melt migration paths indicated by red arrows; near Moho melt sills indicated by red ellipses. Small filled circles depict the exsolution of magmatic volatiles that occurs during differentiation. Sites of axis-centred delivery of mantle melt are more likely to be hydrothermally active and resurfaced frequently by extrusive volcanism (plume and smooth sea floor in top panel). Sites of off-axis delivery of mantle melt sustain greater amounts of tectonic extension, erupt less frequently and host more intermittent high-temperature hydrothermal activity (rougher sea floor in bottom panel).

melt at near-Moho depths and possibly a decrease in temperature. Towards the Siqueiros transform the increase in seismic velocity is most pronounced, consistent with the observed decrease in crustal thickness[19].

Between transform offsets, EPR segments are separated by OSCs or second-order ridge crest discontinuities[3]. The right-stepping 9° 03′ N OSC occurs near the ends of *en echelon* segments of the MLVZ, or where the centre of mantle upwelling is sheared in a right-lateral sense. We suggest that the large-scale azimuthal rotation of mantle upwelling, with respect to the current Euler pole of Pacific–Cocos plate motion, governs the formation and evolution of the OSC (Fig. 4). According to this view, mantle upwellings organize into *en echelon* segments and large-offset OSCs provide an accommodation zone that moves the lithospheric plate boundary from one segment of mantle upwelling to another. A previous hypothesis for the origin of OSCs attributes them to variations in the duration, timing or intensity of magmatic pulses that inflate crustal magma chambers and that propagate along the plate boundary, in which case a reduced magma supply is expected near second-order discontinuities[4]. An alternative model infers that OSCs are entirely lithospheric features that form in response to changes in plate motion[7]. We conclude that the segmentation of the EPR by OSCs is a direct result of *en echelon* upwelling at mantle depths. OSCs thus do not form in response to reduced magma supply, nor is their evolution related to along-axis migration of magmatic pulses away from centres of replenishment towards magma-starved discontinuities. We propose that OSCs form because the geometry of the rigid plate system is inconsistent with the underlying orientation and geometry of asthenospheric upwelling. As the pattern of mantle upwelling evolves, OSCs will respond to maintain their positions where *en echelon* segments of upwelling are sheared in the cross-axis direction. We predict that both the size and the sense of offset of an OSC, as well as its propagation history, will be related to the underlying and evolving pattern of mantle upwelling.

Between transforms and OSCs the EPR is subtly segmented at a scale of ~25 km, referred to as third-order or volcanic segmentation[3,37]. Multidisciplinary studies reveal that volcanic segments are chemically, structurally and geologically distinct. Petrologic data show that lavas erupted within volcanic segments are compositionally similar, yet differences in lava chemistry between volcanic segments can be pronounced[5,12]. Geophysical studies indicate that the centres of volcanic segments are associated with a more pronounced magmatic system at mid- to lower-crustal depths, and increased temperatures within a thermal boundary layer that connects the magmatic and hydrothermal systems[6,14,38]. Near the boundaries of volcanic segments, seismic reflection and tomographic imaging detect abrupt changes in mid- to upper-crustal structure[6,13,14,38,39]. Lastly, seafloor mapping shows that volcanic and tectonic features are also segmented at this scale[37]. The structure of the MLVZ correlates well with previous indicators of third-order segmentation, supporting the hypothesis that volcanic segmentation of the EPR is inherited from variations in mantle melt delivery[5,6,40]. We note that the spacing of volcanic segments is similar to that of diapirs mapped in the Oman ophiolite[41,42]. Additional studies will be necessary to determine whether this is a coincidence or the result of dynamic upwelling.

Ridge activity and skew of mantle upwelling

We find that the state of volcanic and tectonic activity along the ridge correlates with the cross-axis distance to a centre of mantle melt delivery. Above axis-centred delivery of mantle melt (for example, 9° 50′ N), lavas are young and fissure density is decreased[22,43,44]. Where mantle melt arrives off-axis (for example, 9° 30′ N), older lavas and increased fissuring characterize the axial high. Within our study area, the oldest lavas and the highest density of fissured sea floor[22,44] is found where the MLVZ is farthest from the rise crest (9° 20′ N). Axial eruptive styles also differ, with larger volume flows inferred where off-axis delivery of mantle melt occurs[45]. These relations suggest that shorter repose times and smaller eruption volumes may typify volcanoes fed by axis-centred delivery of mantle melt.

The vigour of hydrothermal venting also correlates with the pattern of magma delivery. In regions of axis-centred delivery, high-temperature hydrothermal venting is associated with recent volcanism and vent-supported biologic communities are abundant[22,43,44]. Either more mature vents or a lack of high-temperature vents and a general decrease in the abundance of vent-supported biota[22,43,44] are observed where mantle melt arrives off-axis. A transition from on-axis to off-axis delivery of mantle melt occurs near 9° 37′ N, where a ridge discontinuity separates a volcanic section of the axial high from a tectonic one and demarcates a significant hydrothermal boundary[12]. North of 9° 37′ N, lavas are less evolved (higher MgO content), eruption temperatures are >1,190 °C, hydrothermal venting is usually >350 °C and vent fluids are consistent with derivation from the vapour phase of phase-separated fluids[12,23]. In contrast, south of 9° 37′ N, where mantle melt is delivered off-axis, basalts are more evolved (lower MgO), eruption temperatures are <1,190 °C, hydrothermal venting temperatures are <325 °C and vent fluids are derived from the brine phase of phase-separated fluids[12,23].

Magma plumbing and the segmentation of the EPR

Three significant new findings of our study are that: (1) mantle upwelling and asthenospheric flow are skewed beneath the plate boundary, and thus the delivery of mantle melt is in many places not centred beneath the rise axis; (2) the 9° 03′ N OSC, a second-order discontinuity of the EPR, occurs where *en echelon* segments of mantle upwelling are offset in the cross-axis direction; and (3) between first- and second-order discontinuities the cross-axis offset between a centre of mantle melt delivery and the rise axis correlates with the intensity of rise crest volcanic, hydrothermal and tectonic activity. Building on these results, we propose a new model of magmatic segmentation beneath fast-spreading ridges, illustrated in Fig. 4. In our model the skew of mantle upwelling beneath the plate boundary governs second-order segmentation of the EPR and the intensity of geologic processes occurring within third-order or volcanic segments. Above we discussed the implications of our results for transforms and OSCs.

Away from OSCs and transforms, volcanic segments receive mantle-derived melt from approximately equally spaced centres. In contrast to previous hypotheses, rise-parallel variations in ridge processes are not simply a function of magma supply or the along-axis redistribution of magma away from a mantle source[3,4,9]. Instead, the cross-axis offset between a centre of mantle melt delivery and the associated axial volcano causes axis-parallel changes in ridge crest processes. We illustrate our magma-plumbing model with two cross-sections (Fig. 4). One is through an axis-centred site of mantle melt delivery and a volcano characterized by frequent extrusive volcanism and vigorous seafloor hydrothermal and biologic systems; this is representative of the rise crest near 9° 50′ N (refs 22, 43) (Figs 1 and 4). In contrast, the second cross-section is through an off-axis centre of melt delivery that feeds melt to an axial volcano where seafloor eruptions occur less frequently, surface tectonic extension is greater and seafloor hydrothermal and biologic activity are less intense; this is representative of the rise crest near 9° 30′ N (refs 22, 43, 44).

The contrasting processes at these two sites cannot be attributed to differences in the size and shape of upper crustal magma chambers, which are similar[13]. Nor is it likely that the observed differences in hydrothermal activity can be attributed to near-surface permeability, which is expected to be greater where seafloor fissuring and faulting is greater[44]. We further rule out magma supply as the controlling factor because crustal thickness, and by association the long-term magma supply, is similar at each location[18,19]. We propose that as the cross-axis offset between a centre of mantle melt delivery and the rise crest increases, so does the differentiation of magma that is delivered to the

volcano. With cooling and differentiation, magma changes its composition, increases its density and enhances the exsolution of magmatic volatiles. We infer that such fundamental changes in the qualities of magma will shape near-surface processes driven by crustal magma chambers.

Our model predicts that magma entering the crustal system from an axis-centred site of mantle melt delivery will have undergone relatively less differentiation. Such magma will be higher in temperature, more buoyant (that is, higher MgO) and retain more of its primary volatiles, thus increasing the breaching of the reaction zone above the axial magma chamber, the exchange of energy between the magmatic and hydrothermal systems and the recurrence of extrusive volcanism that localizes vigorous, high-temperature venting and biological activity. Sites of axis-centred delivery of mantle melt are most likely to be characterized as volcanically and hydrothermally robust on the basis of surface geology. In the case of off-axis delivery of mantle melt our model predicts that lateral migration of melt at sub-crustal depths will promote igneous differentiation. Crustal magma reservoirs will thus receive melt that is both cooler and denser (higher FeO) than in reservoirs above axis-centred upwellings. Depending on the degree of differentiation, considerable open-system fractionation of magmatic volatiles could occur off-axis, in which case the rate of pressurization of a ridge-crest magma chamber by volatiles would be lower. A decrease in the volatile content of an axial magma chamber should decrease the breaching of the hydrothermal reaction zone and reduce the frequency of volcanic eruptions. In this setting, localized high-temperature hydrothermal venting may be intermittent and lower-temperature, diffuse-flow venting could prevail. Such characteristics are commonly attributed to magma starvation. In our magma plumbing model, two axial volcanoes (or third-order segments) can receive similar volumes of magma, but behave differently (extrusive versus intrusive) because of sub-crustal, differentiation-induced changes in magma quality.

Previous models of mid-ocean ridges have usually assumed that magma supply controls segmentation, that asthenospheric transport parallels the spreading direction and that mantle upwelling and melt delivery is symmetric about the rise axis. Ours is the first study to show large-scale skew of mantle upwelling beneath mid-ocean ridges and as such it renews the debate over the origin and significance of spreading-centre segmentation. One implication of our results is that local plate motions alone are not the sole cause of sub-ridge mantle flow. On the contrary, the skew of mantle upwelling and transport can act as a driving force for the tectonic reorganization of the EPR and cause along-axis variations in the intensity of ridge-crest processes. We speculate that the skew of the sub-ridge asthenosphere owes its origin to global patterns of mantle flow, which are strongly influenced by the viscous coupling between subducting oceanic slabs and the surrounding mantle. If this speculation holds, it implies that the flux of slabs into the mantle may be linked to the segmentation of mid-ocean ridges.

Received 30 August 2006; accepted 8 February 2007.

1. Whitehead, J. A. Jr, Dick, H. J. B. & Schouten, H. A mechanism for magmatic accretion under spreading centres. *Nature* **312,** 146–148 (1984).
2. Schouten, H., Klitgord, K. D. & Whitehead, J. A. Segmentation of mid-ocean ridges. *Nature* **317,** 225–229 (1985).
3. Macdonald, K. C. *et al.* A new view of the mid-ocean ridge from the behaviour of ridge-axis discontinuities. *Nature* **335,** 217–225 (1988).
4. Macdonald, K. C., Scheirer, D. S. & Carbotte, S. M. Mid-ocean ridges: Discontinuities, segments and giant cracks. *Science* **253,** 986–994 (1991).
5. Langmuir, C. H., Bender, J. F. & Batiza, R. Petrological and tectonic segmentation of the East Pacific Rise, 5°30′-14°30′N. *Nature* **322,** 422–429 (1986).
6. Toomey, D. R., Purdy, G. M., Solomon, S. C. & Wilcock, W. S. D. The three-dimensional seismic velocity structure of the East Pacific Rise near latitude 9°30′N. *Nature* **347,** 639–645 (1990).
7. Lonsdale, P. Segmentation of the Pacific-Nazca Spreading Center, 1°N-20°S. *J. Geophys. Res.* **94,** 12197–12226 (1989).
8. Parmentier, E. M. & Morgan, J. P. Spreading rate dependence of three-dimensional structure in oceanic spreading centers. *Nature* **348,** 325–328 (1990).
9. Bell, R. E. & Buck, W. R. Crustal control of ridge segmentation inferred from observations of the Reykjanes ridge. *Nature* **357,** 583–586 (1992).
10. Sempéré, J.-C. & Macdonald, K. C. Deep-tow studies of the overlapping spreading centers at 9°03′N on the East Pacific Rise. *Tectonics* **5,** 881–900 (1986).
11. Carbotte, S. M. & Macdonald, K. C. East Pacific Rise 8°-10°30′N: Evolution of ridge segments and discontinuities from SeaMARC II and three-dimensional magnetic studies. *J. Geophys. Res.* **97,** 6959–6982 (1992).
12. Smith, M. C. *et al.* Magmatic processes and segmentation at a fast spreading mid-ocean ridge; detailed investigation of an axial discontinuity on the East Pacific Rise crest at 9°37′N. *Geochem. Geophys. Geosyst.* **2,** doi:10.1029/2000GC000134 (2001).
13. Kent, G. M., Harding, A. J. & Orcutt, J. A. Distribution of magma beneath the East Pacific Rise between the Clipperton Transform and the 9°17′N Deval from forward modeling of common depth point data. *J. Geophys. Res.* **98,** 13945–13969 (1993).
14. Dunn, R. A., Toomey, D. R. & Solomon, S. C. Three-dimensional seismic structure and physical properties of the crust and shallow mantle beneath the East Pacific Rise at 9°30′N. *J. Geophys. Res.* **105,** 23537–23555 (2000).
15. Scheirer, D. S. & Macdonald, K. C. Variation in cross-sectional area of the axial ridge along the East Pacific Rise: Evidence for the magmatic budget of a fast spreading center. *J. Geophys. Res.* **98,** 7871–7885 (1993).
16. Detrick, R. S. *et al.* Multi-channel seismic imaging of a crustal magma chamber along the East Pacific Rise. *Nature* **326,** 35–41 (1987).
17. Vera, E. E. *et al.* The structure of 0- to 0.2-m.y.-old oceanic crust at 9°N on the East Pacific Rise from expanded spread profiles. *J. Geophys. Res.* **95,** 15529–15556 (1990).
18. Barth, G. A. & Mutter, J. C. Variability in oceanic crustal thickness and structure: Multichannel seismic reflection results from the northern East Pacific Rise. *J. Geophys. Res.* **101,** 17951–17975 (1996).
19. Canales, J. P., Detrick, R. S., Toomey, D. R. & Wilcock, W. S. D. Segment-scale variations in the crustal structure of 150–300 kyr old fast spreading oceanic crust (East Pacific Rise, 8°15′N-10°5′N) from wide-angle seismic refraction profiles. *Geophys. J. Int.* **152,** 766–794 (2003).
20. Batiza, R. & Niu, Y. Petrology and magma chamber processes at the East Pacific Rise ~9°30′N. *J. Geophys. Res.* **97,** 6779–6797 (1992).
21. Perfit, M. R. *et al.* Small-scale spatial and temporal variations in mid-ocean ridge crest magmatic processes. *Geology* **22,** 375–379 (1994).
22. Haymon, R. M. *et al.* Hydrothermal vent distribution along the East Pacific Rise crest (9°09′-54′N) and its relationship to magmatic and tectonic processes on fast-spreading mid-ocean ridges. *Earth Planet. Sci. Lett.* **102,** 513–534 (1991).
23. Von Damm, K. L. Chemistry of hydrothermal vent fluids from 9°-10°, East Pacific Rise: ''Time zero,'' the intermediate posteruptive period. *J. Geophys. Res.* **105,** 11203–11222 (2000).
24. Gripp, A. E. & Gordan, R. G. Young tracks of hotspots and current plate velocities. *Geophys. J. Int.* **150,** 321–361 (2002).
25. Key, K. & Constable, S. Mantle upwelling beneath the East Pacific Rise at 9°30′N. *Eos* (Fall Meet. Suppl.) **87** (52), abstr. B31B–1114 (2006).
26. Crawford, W. C. & Webb, S. C. Variations in the distribution of magma in the lower crust and at the Moho beneath the East Pacific Rise at 9°-10°N. *Earth Planet. Sci. Lett.* **203,** 117–130 (2002).
27. Singh, S. C. *et al.* Seismic reflection images of the Moho underlying melt sills at the East Pacific Rise. *Nature* **442,** 287–290 (2006).
28. Kent, G. M. *et al.* Evidence from three-dimensional seismic reflectivity images for enhanced melt supply beneath mid-ocean-ridge discontinuities. *Nature* **406,** 614–618 (2000).
29. Dunn, R. A., Toomey, D. R., Detrick, R. S. & Wilcock, W. S. D. Continuous mantle melt supply beneath an overlapping spreading center on the East Pacific Rise. *Science* **291,** 1955–1958 (2001).
30. Faul, U. H., Toomey, D. R. & Waff, H. S. Intergranular basaltic melt is distributed in thin, elongated inclusions. *Geophys. Res. Lett.* **21,** 29–32 (1994).
31. Hammond, W. C. & Humphreys, E. D. Upper mantle seismic wave velocity: Effects of realistic partial melt geometries. *J. Geophys. Res.* **105,** 10975–10986 (2000).
32. Nicolas, A. & Christensen, N. I. in *Composition, Structure, and Dynamics of the Lithosphere-Asthenosphere System* (eds Fuchs, K. & Froidevaux, C.) 111–123 (American Geophysical Union, Washington DC, 1987).
33. Ben Ismaïl, W. & Mainprice, D. An olivine fabric database: an overview of upper mantle fabrics and seismic anisotropy. *Tectonophysics* **296,** 145–157 (1998).
34. Blackman, D. K., Wenk, H.-R. & Kendall, J. M. Seismic anisotropy of the upper mantle: 1. Factors that affect mineral texture and effective elastic properties. *Geochem. Geophys. Geosyst.* **3,** doi:10.1029/2001GC000248 (2002).
35. Pockalny, R. A., Fox, P. J., Fornari, D. J., Macdonald, K. C. & Perfit, M. R. Tectonic reconstruction of the Clipperton and Siqueiros Fracture Zones: Evidence and consequences of plate motion change for the last 3 Myr. *J. Geophys. Res.* **102,** 3167–3181 (1997).
36. Richards, M. A. & Lithgow-Bertelloni, C. Plate motion changes, the Hawaiian-Emperor bend, and the apparent success and failure of geodynamic models. *Earth Planet. Sci. Lett.* **137,** 19–27 (1996).
37. White, S. M., Haymon, R. M., Fornari, D. J., Perfit, M. R. & Macdonald, K. C. Correlation between volcanic and tectonic segmentation of fast-spreading ridges: Evidence from volcanic structures and lava flow morphology on the East Pacific Rise at 9°-10°N. *J. Geophys. Res.* **107,** doi:10.1029/2001JB000571 (2002).
38. Toomey, D. R., Solomon, S. C. & Purdy, G. M. Tomographic imaging of the shallow crustal structure of the East Pacific Rise at 9°30′N. *J. Geophys. Res.* **99,** 24135–24157 (1994).

39. Tian, T., Wilcock, W. S. D., Toomey, D. R. & Detrick, R. S. Seismic heterogeneity in the upper crust near the 1991 eruption site on the East Pacific Rise. *Geophys. Res. Lett.* **27,** 2369–2372 (2000).
40. Dunn, R. A. & Toomey, D. R. Seismological evidence for three-dimensional melt migration beneath the East Pacific Rise. *Nature* **388,** 259–262 (1997).
41. Nicolas, A. *Structures of Ophiolites and Dynamics of Oceanic Lithosphere* 70–77 (ed. Nicolas, A.) (Kluwer Academic, Dordrecht, 1989).
42. Jousselin, D., Nicolas, A. & Boudier, F. Detailed mapping of a mantle diapir below a paleo-spreading center in the Oman ophiolite. *J. Geophys. Res.* **103,** 18153–18170 (1998).
43. Fornari, D. J., Haymon, R. M., Perfit, M. R., Gregg, T. K. P. & Edwards, M. H. Axial summit trough of the East Pacific Rise 9°-10°N: Geological constraints and evolution of the axial zone of fast spreading mid-ocean ridges. *J. Geophys. Res.* **103,** 9827–9855 (1998).
44. Wright, D. J., Haymon, R. M. & Fornari, D. J. Crustal fissuring and its relationship to magmatic and hydrothermal processes on the East Pacific Rise crest (9°12′ to 54′N). *J. Geophys. Res.* **100,** 6097–6120 (1995).
45. Soule, S. A. *et al.* Channelized lava flows at the East Pacific Rise crest 9°-10°N: The importance of off-axis lava transport in developing the architecture of young oceanic crust. *Geochem. Geophys. Geosyst.* **6,** doi:10.1029/2005GC000912 (2005).

Supplementary Information is linked to the online version of the paper at www.nature.com/nature.

Acknowledgements We thank the officers and crew of the RV *Maurice Ewing* and members of the scientific party for their assistance. D.R.T. thanks E. Hooft and E. Humphreys for numerous discussions and J. Karson, T. Durant and D. Villagomez for comments. Supported by the RIDGE and RIDGE 2000 Programs, Ocean Sciences Division, NSF.

Author Contributions All authors participated in the experimental design, the collection of the data and in several stages of data reduction and analysis. D.R.T. conducted the tomographic analysis and wrote the manuscript with comments from co-authors.

Author Information Reprints and permissions information is available at www.nature.com/reprints. The authors declare no competing financial interests. Correspondence and requests for materials should be addressed to D.R.T. (drt@uoregon.edu).